Preparation of Fluorescent Diamond Nanoparticles Stably Dispersed under a Physiological Environment through Multistep Organic Transformations

Tatsuya Takimoto,[†] Tokuhiro Chano,[‡] Sawako Shimizu,[‡] Hidetoshi Okabe,[‡] Masaaki Ito,[§] Masahito Morita,[⊥,#] Takahide Kimura,[†] Toshiro Inubushi,[‖] and Naoki Komatsu*,[†]

[†]*Department of Chemistry, Shiga University of Medical Science, Seta, Otsu 520-2192, Japan,* [‡]*Department of Clinical Laboratory Medicine, Shiga University of Medical Science, Seta, Otsu 520-2192, Japan,* [§]*Organic Chemical Company, Daicel Chemical Industries, Ltd., 2-1-4 Higashisakae, Ohtake, Hiroshima 739-0605, Japan,* [⊥]*Immunology Frontier Research Center, Osaka University, 3-1 Yamadaoka, Suita 565-0871, Japan,* [#]*PRESTO, JST, 4-1-8, Honcho, Kawaguchi-shi, Saitama, 332-0012, Japan, and* [‖]*Biomedical MR Science Center, Shiga University of Medical Science, Seta, Otsu 520-2192, Japan*

Received February 24, 2010. Revised Manuscript Received April 8, 2010

Imparting multiple functions to nanoparticles through organic functionalization has been attracting significant interest, particularly in terms of biomedical applications. Among them, diamond nanoparticles—the so-called nanodiamond (ND)—have been recognized as one of the best platforms, because of its nontoxic or low-toxicity properties, as well as its organic characteristics that enable covalent bonding with introduced functionalities. Here, we show multistep organic transformations on the ND surface that amass the requisite functions layer by layer through covalent bonds. The functionalities introduced onto the ND surface were well-characterized by solution-phase ^{1}H NMR and ^{13}C NMR spectroscopies, recently developed by us and other groups, as well as conventional infrared (IR), fluorescence microscopy and spectroscopy, and elemental analysis. As a result, hydrophilic and fluorescent characteristics were incorporated onto the ND surface by adding polyethylene glycol (PEG) and fluorescein segments, providing fluorescent ND stably dispersed under a physiological environment. ND has been confirmed to be viable for use as a cellular imaging agent by introducing them into HeLa cells.

Introduction

Biomedical applications of nanoparticles have attracted growing interest, because of the high potential for early diagnosis and targeted therapeutics.[1−8] In particular, various inorganic nanoparticles made from gold, silica, iron oxide, manganese oxide, and cadmium selenide (quantum dots) are frequently used as platforms for biomedical imaging[9] or drug delivery,[10,11] mainly because of the availability of the size-controlled particles,[12−14] and/or their characteristic magnetic and optical properties.[15−17] However, in view of their clinical use, more functions should be programmed into the nanoparticles, such as in vivo dispersibility, target specificity, controlled release, and multiple imaging modalities. Therefore, appropriate organic functionalities are frequently required to be immobilized on the surface of the nanoparticles to add more and tunable functions for nanoparticles. However, methods of chemical functionalization onto the inorganic (noncarbonaceous) nanoparticles are limited; reliable methods to construct the interfacial connections between inorganic core and organic functionalities have been confined mostly to sol−gel reactions of silica nanoparticles,[18] lipid coating of

*Author to whom correspondence should be addressed. Tel.: +81-77-548-2102. Fax: +81-77-548-2405. E-mail address: nkomatsu@belle.shiga-med.ac.jp.

(1) De, M.; Ghosh, P. S.; Rotello, V. M. *Adv. Mater.* **2008,** *20,* 4225–4241.
(2) Rao, J. *ACS Nano* **2008,** *2,* 1984–1986.
(3) Emerrich, D. F.; Thanos, C. G. *J. Drug Targeting* **2007,** *15,* 163–183.
(4) Caruthers, S. D.; Wickline, S. A.; Lanza, G. M. *Curr. Opin. Biotechnol.* **2007,** *18,* 26–30.
(5) Farokhzad, O. C.; Langer, R. *Adv. Drug Delivery Rev.* **2006,** *58,* 1456–1459.
(6) Gil, P. R.; Parak, W. J. *ACS Nano* **2008,** *2,* 2200–2205.
(7) Liu, Y.; Miyoshi, H.; Nakamura, M. *Int. J. Cancer* **2007,** *120,* 2527–2537.
(8) Jain, K. K. *Clin. Chim. Acta* **2005,** *358,* 37–54.
(9) Cheon, J.; Lee, J.-H. *Acc. Chem. Res.* **2008,** *41,* 1630–1640.
(10) Farokhzad, O. C.; Langer, R. *ACS Nano* **2009,** *3,* 16–20.
(11) Peer, D.; Karp, J. M.; Hong, S.; Farokhzad, O. C.; Margalit, R.; Langer, R. *Nature Nanotechnol.* **2007,** *2,* 751–760.
(12) Tao, A. R.; Habas, S.; Yang, P. *Small* **2008,** *4,* 310–325.
(13) Skrabalak, S. E.; Xia, Y. *ACS Nano* **2009,** *3,* 10–15.
(14) Zhang, Q.; Xie, J.; Yang, J.-H.; Lee, J. Y. *ACS Nano* **2009,** *3,* 139–148.
(15) Cai, W.; Chen, X. *Small* **2007,** *3,* 1840–1854.
(16) Douma, K.; Prinzen, L.; Slaaf, D. W.; Reutelingsperger, C. P. M.; Biessen, E. A. L.; Hackeng, T. M.; Post, M. J.; van Zandvoort, M. A. M. J. *Small* **2009,** *5,* 544–557.
(17) Rogach, A. L.; Gaponik, N.; Lupton, J. M.; Bertoni, C.; Gallardo, D. E.; Dunn, S.; Pira, N. L.; Paderi, M.; Repetto, P.; Romanov, S. G.; O'Dwyer, C.; Torres, C. M. S.; Eychmüller, A. *Angew. Chem., Int. Ed.* **2008,** *47,* 6538–6549.
(18) Jamieson, T.; Bakhshi, R.; Petrova, D.; Pocock, R.; Imani, M.; Seifalian, A. M. *Biomaterials* **2007,** *28,* 4717–4732.

Article

Chem. Mater., Vol. 22, No. 11, 2010 3463

hydrophobic nanoparticles,[19] and ligation of thiol to metallic nanoparticles.[20]

In contrast, carbon nanomaterials such as carbon nanotubes, fullerenes, and, quite recently, nanographene have been functionalized covalently in various ways, thanks to their organic characteristics.[21−23] Although carbon materials are classified as inorganic, their behaviors toward organic functionalization are different from noncarbonaceous materials. Diamond is also categorized as an inorganic material, because of its robustness and chemical stability. Many organic reactions have been applied to form covalent bonds between the diamond surface and the functionalities[24−27] both in film[28−36] and nanometer-sized particles.[37−45] The chemically inert but functionalizable characteristics of diamond have been recently applied to the synthesis of diamond-based biosensors[32] and DNA chips.[31,33,46] Diamond has gradually taken on organic characteristics, as well as fullerenes and carbon nanotubes.[47]

Diamond nanoparticles—the so-called nanodiamond (ND)—have been recently attracting significant interest in their biological and medicinal applications, mainly because of their nontoxic or low-toxicity properties, as well as their above-mentioned organic characteristics. Various types of fluorescent ND have already been prepared physically by ion implantation[48−56] and chemically by organic functionalization,[57−60] and they have been introduced into cells, exhibiting almost no cytotoxicity. However, NDs ($\sim$50 and 5 nm in size) have been reported to form unstable hydrosols without the aid of a surfactant and precipitate under a physiological environment (for example, in phosphate buffer saline (PBS)).[59,61,62] We also have observed similar phenomena, as will be mentioned below (Figure 7). In view of further extensions of the biomedical applications, a stable hydrosol of ND should be produced by surface modification, as noted in the review articles recently written by Shenderova[61] and Dai.[63] In addition, an increasing number of excellent papers have appeared in recent years on the subject of covalent chemical functionalization and characterization of NDs,[50,57,59,60,64−67] which has prompted us to report our results.

(19) van Schooneveld, M. M.; Vucic, E.; Koole, R.; Zhou, Y.; Stocks, J.; Cormode, D. P.; Tang, C. Y.; Gordon, R. E.; Nicolay, K.; Meijerink, A.; Fayad, Z. A.; Mulder, W. J. M. *Nano Lett.* **2008**, *8*, 2517–2525.
(20) Templeton, A. C.; Wuelfing, W. P.; Murray, R. W. *Acc. Chem. Res.* **2000**, *33*, 27–36.
(21) Peng, X.; Wong, S. S. *Adv. Mater.* **2009**, *21*, 625–642.
(22) Liu, Z.; Robinson, J. T.; Sun, X.; Dai, H. *J. Am. Chem. Soc.* **2008**, *130*, 10876–10877.
(23) Liu, Z.; Sun, X.; Nakayama-Ratchford, N.; Dai, H. *ACS Nano* **2007**, *1*, 50–56.
(24) Krueger, A. *Chem.—Eur. J.* **2008**, *14*, 1382–1390.
(25) Krueger, A. *Adv. Mater.* **2008**, *20*, 2445–2449.
(26) Krueger, A. *J. Mater. Chem.* **2008**, *18*, 1485–1492.
(27) Holt, K. B. *Philos. Trans. R. Soc. A* **2007**, *365*, 2845–2861.
(28) Nebel, C. E.; Shin, D.; Rezek, B.; Tokuda, N.; Uetsuka, H.; Watanabe, H. *J. R. Soc. Interface* **2007**, *4*, 439–461.
(29) Zhong, Y. L.; Loh, K. P.; Midya, A.; Chen, Z.-K. *Chem. Mater.* **2008**, *20*, 3137–3144.
(30) Rezek, B.; Shin, D.; Nakamura, T.; Nebel, C. E. *J. Am. Che, Soc.* **2006**, *128*, 3884–3885.
(31) Kuga, S.; Yang, J.-H.; Takahashi, H.; Hirama, K.; Iwasaki, T.; Kawarada, H. *J. Am. Chem. Soc.* **2008**, *130*, 13251–13263.
(32) Härtl, A.; Schmich, E.; Garrido, J. A.; Hernando, J.; Catharino, S. C. R.; Walter, S.; Feulner, P.; Kromka, A.; Steinmüller, D.; Stutzmann, M. *Nat. Mater.* **2004**, *3*, 736–742.
(33) Yang, W.; Auciello, O.; Butler, J. E.; Cai, W.; Carlisle, J. A.; Gerbi, J.; Gruen, D. M.; Knickerbocker, T.; Lasseter, T.; Russell, J. N., Jr.; Smith, L. M.; Hamers, R. J. *Nat. Mater.* **2002**, *1*, 253–257.
(34) Smentkowski, V. S.; Yates, J. T., Jr. *Science* **1996**, *271*, 193–195.
(35) Nakamura, T.; Suzuki, M.; Ishihara, M.; Ohana, T.; Tanaka, A.; Koga, Y. *Langmuir* **2004**, *20*, 5846–5849.
(36) Hovis, J. S.; Coulter, S. K.; Harmers, R. J. *J. Am. Chem. Soc.* **2000**, *122*, 732–733.
(37) Nakamura, T.; Ishihara, M.; Ohana, T.; Koga, Y. *Chem. Commun.* **2003**, 900–901.
(38) Li, L.; Davidson, J. L.; Lukehart, C. M. *Carbon* **2006**, *44*, 2308–2315.
(39) Liu, Y.; Gu, Z.; Margrave, J. L.; Khabashesku, V. N. *Chem. Mater.* **2004**, *16*, 3924–3930.
(40) Miller, J. B.; Brown, D. W. *Langmuir* **1996**, *12*, 5809–5817.
(41) Saito, T.; Ikeda, Y.; Egawa, S.; Kusakabe, K.; Morooka, S.; Maeda, H.; Taniguchi, Y.; Fujiwara, Y. *J. Chem. Soc. Faraday Trans.* **1998**, *94*, 929–932.
(42) Ushizawa, K.; Sato, Y.; Mitsumori, T.; Machinami, T.; Ueda, T.; Ando, T. *Chem. Phys. Lett.* **2002**, *351*, 105–108.
(43) Tsubota, T.; Urabe, K.; Egawa, S.; Takagi, H.; Kusakabe, K.; Morooka, S.; Maeda, H. *Diamond Relat. Mater.* **2000**, *9*, 219–223.
(44) Tsubota, T.; Tanii, S.; Ida, S.; Nagata, M.; Matsumoto, Y. *Phys. Chem. Chem. Phys.* **2003**, *5*, 1474–1480.
(45) Tsubota, T.; Hirabayashi, O.; Ida, S.; Nagaoka, G.; Nagata, M.; Matsumoto, Y. *Phys. Chem. Chem. Phys.* **2002**, *4*, 806–811.
(46) Yang, N.; Uetsuka, H.; Osawa, E.; Nebel, C. E. *Angew. Chem., Int. Ed.* **2008**, *47*, 5183–5185.
(47) Schwertfeger, H.; Fokin, A. A.; Schreiner, P. R. *Angew. Chem., Int. Ed.* **2008**, *47*, 1022–1036.
(48) Vaijayanthimala, V.; Chang, H.-C. *Nanomedicine* **2009**, *4*, 47–55.
(49) Mohan, N.; Tzeng, Y.-K.; Yang, L.; Chen, Y.-Y.; Hui, Y. Y.; Fang, C.-Y.; Chang, H.-C. *Adv. Mater.* **2010**, *22*, 843–847.
(50) Zhang, B.; Li, Y.; Fang, C.-Y.; Chang, C.-C.; Chen, C.-S.; Chen, Y.-Y.; Chang, H.-C. *Small* **2009**, *5*, 2716–2721.
(51) Chang, Y.-R.; Lee, H.-Y.; Chen, K.; Chang, C.-C.; Tsai, D.-S.; Fu, C.-C.; Lim, T.-S.; Tzeng, Y.-K.; Fang, C.-Y.; Han, C.-C.; Chang, H.-C.; Fann, W. *Nature Nanotechnol.* **2008**, *3*, 284–288.
(52) Tisler, J.; Balasubramanian, G.; Naydenov, B.; Kolesov, R.; Grotz, B.; Reuter, R.; Boudou, J. P.; Curmi, P. A.; Sennour, M.; Thorel, A.; Börsch, M.; Aulenbacher, K.; Erdmann, R.; Hemmer, P. R.; Jelezko, F.; Wrachtrup, J. *ACS Nano* **2009**, *3*, 1959–1965.
(53) Faklaris, O.; Joshi, V.; Irinopoulou, T.; Tauc, P.; Sennour, M.; Girard, H.; Gesset, C.; Arnault, J.-C.; Thorel, A.; Boudou, J. P.; Curmi, P. A.; Treussart, F. *ACS Nano* **2009**, *3*, 3955–3962.
(54) Faklaris, O.; Garrot, D.; Joshi, V.; Druon, F.; Boudou, J.-P.; Sauvage, T.; Georges, P.; Curmi, P. A.; Treussart, F. *Small* **2008**, *4*, 2236–2239.
(55) Chang, I. P.; Hwang, K. C.; Chiang, C.-S. *J. Am. Chem. Soc.* **2008**, *130*, 15476–15481.
(56) Chao, J.-I.; Perevedentseva, E.; Chung, P.-H.; Liu, K.-K.; Cheng, C.-Y.; Chang, C.-C.; Cheng, C.-L. *Biophys. J.* **2007**, *93*, 2199–2208.
(57) Martin, R.; Alvaro, M.; Herance, J. R.; Garcia, H. *ACS Nano* **2010**, *4*, 65–74.
(58) Loh, O.; Lam, R.; Chen, M.; Moldovan, N.; Huang, H.; Ho, D.; Espinosa, H. D. *Small* **2009**, *5*, 1667–1674.
(59) Hens, S. C.; Cunningham, G.; Tyler, T.; Moseenkov, S.; Kuznetsov, V.; Shenderova, O. *Diamond Relat. Mater.* **2008**, *17*, 1858–1866.
(60) Vial, S.; Mansuy, C.; Sagan, S.; Irinopoulou, T.; Burlina, F.; Boudou, J. P.; Chassaing, G.; Lavielle, S. *ChemBioChem* **2008**, *9*, 2113–2119.
(61) Schrand, A. M.; Hens, S. A. C.; Shenderova, O. A. *Crit. Rev. Solid State Mater. Sci.* **2009**, *34*, 18–74.
(62) Pyzyr, A. P.; Bondar, V. S.; Bukayemsky, A. A.; Selyutin, G. E.; Kargin, V. F. In *Synthesis, Properties and Applications of Ultra-nanocrystalline Diamond*; Gruen, D. M., Shenderova, O. A., Vul', A. Y., Eds.; NATO Science Series II Mathematics, Physics and Chemistry; Springer: Dordrecht, The Netherlands, 2005; pp 261−270.
(63) Xing, Y.; Dai, L. *Nanomedicine* **2009**, *4*, 207–218.
(64) Martin, R.; Heydorn, P. C.; Alvaro, M.; Garcia, H. *Chem. Mater.* **2009**, *21*, 4505–4514.
(65) Mochalin, V. N.; Gogotsi, Y. *J. Am. Chem. Soc.* **2009**, *131*, 4594–4595.
(66) Yeap, W. S.; Tan, Y. Y.; Loh, K. P. *Anal. Chem.* **2008**, *80*, 4659–4665.
(67) Cheng, J.; He, J.; Li, C.; Yang, Y. *Chem. Mater.* **2008**, *20*, 4224–4230.
(68) Komatsu, N. *J. Incl. Phenom. Macrocycl. Chem.* **2008**, *61*, 195–216.
(69) Peng, X.; Komatsu, N.; Kimura, T.; Osuka, A. *ACS Nano* **2008**, *2*, 2045–2050.

Scheme 1. Synthetic Route from Hydrogenated ND 1 to Fluorescent ND 3

Scheme 2. Synthesis of Nanodiamondyl Aminododecanoate 6 from 1 via Routes A and B
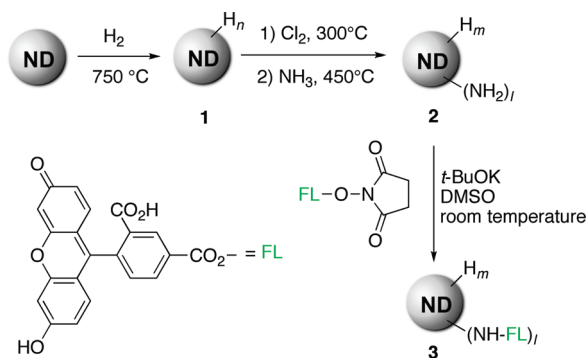
In continuation of our effort to apply organic chemistry to carbon nanomaterials,[68−72] we conducted multistep organic transformations on an ND surface to impart hydrophilic and fluorescent characteristics one by one. In each step of the functionalizations, the product was characterized primarily with solution-phase ^{1}H NMR and ^{13}C NMR spectroscopies, as well as infrared (IR), elemental analysis, and fluorescence microscopy and spectroscopy. The solution-phase NMR technique is much more convenient and informative than a solid-phase one. It is a novel method for analyzing suspended nanoparticles and is found to be applicable to relatively large sizes of nanoparticles (~30 nm).[38,64,72,73] Eventually, we synthesized fluorescent ND that was stably dispersed under a physiological environment and applied it to fluorescence cell imaging.

Results and Discussion

Since the labeling agents are frequently bound to biological entities through amide linkage by reaction of primary amine with carboxylic acid or its derivatives, we attempted to prepare fluorescent ND **3** from hydrogenated ND **1** via amino-functionalized ND **2**, as shown in Scheme 1.[74,75] Although various reaction conditions were examined for the incorporation of fluorescein to **2** through amide linkage, no clear fluorescence was observed from the product **3**, as shown in the fluorescence image (see Figure S1a in the Supporting Information), and almost no difference on the IR spectra was observed between **2** and **3** (see Figure S1b in the Supporting Information). These results indicate that little or no fluorescein was introduced to the ND. This may be attributed to steric hindrance on the ND surface, to prevent fluorescein from approaching to the amino groups. Therefore, we designed another precursor
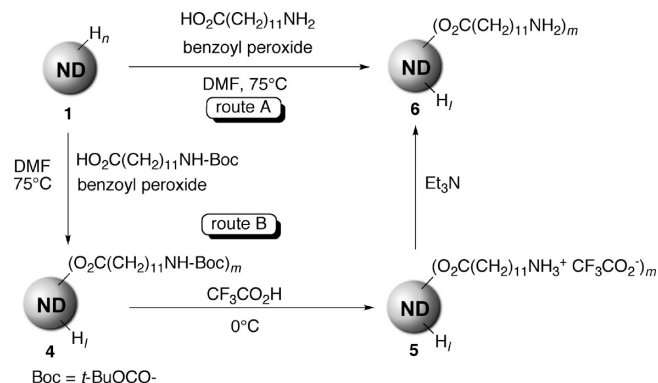
for fluorescent ND that possesses amino groups apart from the ND surface, which fluorescein can freely access.

While nonblinking and nonbleaching fluorescence from ND has been prepared by ion implantation and utilized extensively for cell labeling,[48,50−56] fluorophore-immobilized ND is considered to possess the following advantages: (i) specific instrumentation for ion implantation is not required to make the ND fluoresce, and (ii) emission and excitation wavelengths can be tuned by choosing an appropriate fluorophore.[57,61]

Synthesis and Characterization of Aminododecanoate of ND. A radical reaction of hydrogenated ND with carboxylic acid was chosen to bind ω-amino acid on **1** through ester linkage (see Scheme 2).[44,45] We chose this reaction for the following two reasons:

(1) The very simple structure of **1**, which consists solely of C (sp^3) and H atoms connected by single bonds (C−C and C−H), facilitates the characterization of the product in each step of the organic transformations by IR (Figure 1),[74] NMR (Figure 2),[72] and elemental analysis (Table 1).

(2) The hydrogen-terminated surface in **1** can largely reduce the possibility of physisorption of the reactants onto the ND surface.[76]

In addition to the direct route to **6** through the reaction of ω-aminododecanoic acid with **1** (route A in Scheme 2), Boc (*t*-butoxycarbonyl)-protected ω-aminododecanoic acid was also employed (route B). Spectroscopic and elemental analyses enabled qualitative and quantitative characterization of products **4** and **6**. In particular, solution-phase NMR spectroscopy realized convenient and informative analysis of the organically functionalized nanoparticle.[38,64,72,73]

In the IR spectra of **6-A** and **6-B**, prepared via routes A and B, respectively, the absorptions corresponding to N−H stretching, C−H stretching, C=O stretching, and N−H bending are observed at 3400, 2900, 1710, and 1650 cm^{-1}, respectively, indicating the formation of **6** (Figure 1). On the basis of the absorbance of C−H stretching at 2900 cm^{-1}, the relative intensity corresponding to N−H at 3400 and 1650 cm^{-1} in **6-B** is larger than that in **6-A**, indicating that **6-B** is more functionalized with ω-aminododecanoate than **6-A**.

(70) Peng, X.; Komatsu, N.; Kimura, T.; Osuka, A. *J. Am. Chem. Soc.* **2007**, *129*, 15947–15953.

(71) Peng, X.; Komatsu, N.; Bhattacharya, S.; Shimawaki, T.; Aonuma, S.; Kimura, T.; Osuka, A. *Nature Nanotechnol.* **2007**, *2*, 361–365.

(72) Komatsu, N.; Kadota, N.; Kimura, T.; Osawa, E. *Chem. Lett.* **2007**, *36*, 398–399.

(73) Korokov, V. V.; Kulakova, I. I.; Tarasevich, B. N.; Lisichkin, G. V. *Diamond Relat. Mater.* **2007**, *16*, 2129–2132.

(74) Ando, T.; Ishii, M.; Kamo, M.; Sato, Y. *J. Chem. Soc. Faraday Trans.* **1993**, *89*, 1783–1789.

(75) Ando, T.; Yamamoto, K.; Suehara, S.; Kamo, M.; Sato, Y.; Shimosaki, S.; Nishitani-Gamo, M. *J. Chin. Chem. Soc.* **1995**, *42*, 285–292.

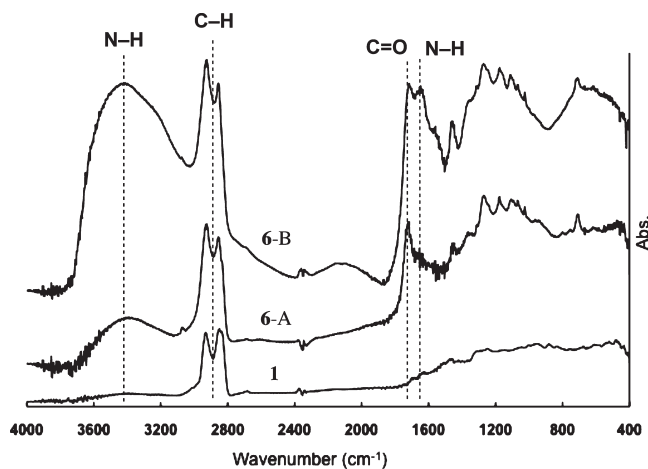(76) Huang, L.-C. L.; Chang, H.-C. *Langmuir* **2004**, *20*, 5879–5884.
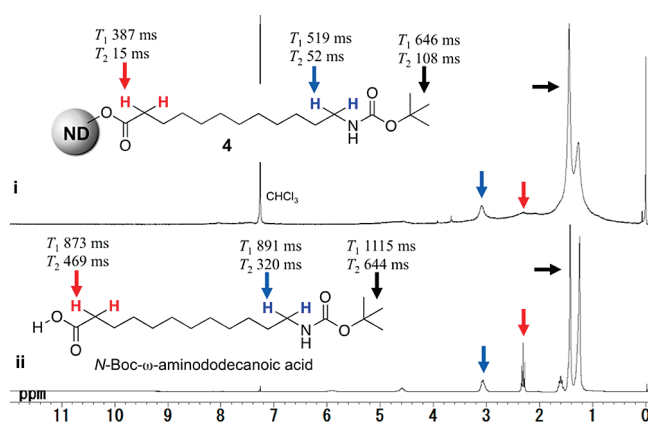
Figure 1. Infrared (IR) spectra of **1**, **6-A**, and **6-B**.

Figure 2. Solution-phase ^{1}H NMR spectra of (i) **4** and (ii) *N*-Boc-ω-aminododecanoic acid in CDCl$_3$. The relaxation times (T_1 and T_2) of *t*-Bu at 1.4 ppm (black arrow) and CH$_2$ at 2.3 ppm (red arrow) and CH$_2$ at 3.0 ppm (blue arrow) are indicated at the structures of **4** and *N*-Boc-ω-aminododecanoic acid.

Despite the estimated size being > 30 nm, **4** was well-dispersed in chloroform. Therefore, solution-phase ^{1}H NMR spectroscopy was measured in CDCl$_3$ at room temperature (see Figure 2) and found to give slightly broad, but sufficiently resolved signals for the characterization of **4**. In comparison with the ^{1}H NMR spectrum of *N*-Boc-ω-aminododecanoic acid (Figure 2ii), the corresponding resonances were observed at almost the same chemical shifts in the spectrum of Figure 2i, although they were broadened, probably because of shorter relaxation time and/or magnetic field inhomogeneity caused by differences in magnetic susceptibility between the solid particle and the liquid medium. In fact, the degree of broadening in the resonances correlates qualitatively to that of shortening in relaxation time, as shown in Figure 2. The same chemical shifts of the resonances on the spectra of Figures 2i and 2ii, mentioned above, indicate no anionic characteristics at the carboxylic function (namely carboxylate) and, therefore, no electrostatic interaction between the carboxylate and the hydrogenated ND surface. This is because the carboxylate makes the resonance of the adjacent hydrogens—highlighted by red arrows in the figures—shift upfield, which was confirmed by titration of triethylamine to *N*-Boc-ω-aminododecanoic acid in CDCl$_3$.

Covalent bonding between ND and the *N*-Boc-ω-aminododecanoate moiety was confirmed by the differences in the relaxation times (T_1 and T_2) between the hydrogens at the following three positions, as shown in Figure 2: (CH$_3$)$_3$C− (black arrow), −CH$_2$−NHCO− (blue arrow), and OCO−CH$_2$− (red arrow). All the T_1 and T_2 values (spin−lattice and spin−spin relaxation times, respectively) at the above positions in **4** are smaller than those in the *N*-Boc-ω-aminododecanoic acid. In addition, they become smaller (646 ms → 519 ms → 387 ms in T_1 and 108 ms → 52 ms → 15 ms in T_2), as the position of the hydrogens become closer to the ester group in the following order: (CH$_3$)$_3$C−, −CH$_2$−NHCO−, OCO−CH$_2$−. On the other hand, *N*-Boc-ω-aminododecanoic acid shows similar T_1 and T_2 values in these three types of hydrogens. The relaxation time studies suggest that (i) the mobility of *N*-Boc-ω-aminododecanoic acid was largely restricted after the reaction with ND and (ii) the mobility around the *C*-terminus (−CH$_2$CO$_2$−) is less than that around the *N*-terminus (−CH$_2$NHCO$_2$t-Bu). Therefore, we conclude that *N*-Boc-ω-aminododecanoic acid was firmly immobilized onto the ND surface through ester linkage. A remarkable site-specific reduction in T_2 (469 ms →15 ms) at OCO−CH$_2$− may provide another support for the ester linkage onto the ND surface; that is, ND intrinsically includes spins (unpaired electrons)[77,78] and the electron spins near ND surface are considered to significantly accelerate the relaxation (T_2) of nuclear spins of hydrogens close to the ND surface through spin−spin interaction. In the solution-phase ^{13}C NMR of **4** (shown in Figure S2 in the Supporting Information), a broad resonance that originated from the diamond carbons was observed at 34 ppm,[72] along with a resonance assigned to (CH$_3$)$_3$C− at 28 ppm. These observations on the NMR spectra lead to the conclusion that the aminododecanoate moiety connects covalently to the ND surface through ester linkage.

To our knowledge, this is one of the largest nanoparticles giving clear NMR spectra in the solution phase, while a smaller size of ND (∼5 nm) was reported to provide NMR spectra in solution phase.[38,64,67,72,73] Although solid-phase NMR spectroscopy has been frequently used for characterization of carbon materials, it is not so convenient for taking spectra with sufficient sensitivity and resolution, especially in the case of characterization of the organic moiety bound to a particle. In addition, the spectra obtained are not as informative as solution-phase NMR. Herein, it is disclosed that solution-phase NMR can be applied to characterize the surface chemical structures of relatively large nanoparticles.

Although IR spectra in Figure 1 derived a qualitative conclusion of route B as a more efficient route in the synthesis of **6**, the coverage of an ND surface with ω-aminododecanoate was evaluated quantitatively with elemental analysis (Table 1). The introduction of aminododecanoate increases the H, N, and O contents and

(77) Loubser, J.; Wyk, J. *Rep. Prog. Phys.* **1978**, *41*, 1201–1248.
(78) Dubois, M.; Guérin, K.; Petit, E.; Batisse, N.; Hamwi, A.; Komatsu, N.; Giraudet, J.; Pirotte, P.; Masin, F. *J. Phys. Chem. C* **2009**, *113*, 10371–10378.

Table 1. Elemental Analyses of 1, 6-A, and 6-B, and the Estimated Atom Numbers

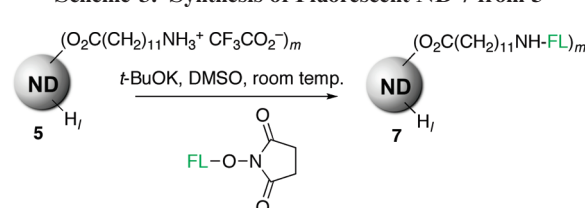|	**1**		**6-A**		**6-B**	
element	composition (wt %)	number of atoms[a]	composition (wt %)	number of atoms[a]	composition (wt %)	number of atoms[a]
H	0.77	2.3×10^5	1.22	3.8×10^5	1.35	4.2×10^5
C	98.5	2.5×10^6	97.2	2.5×10^6	96.4	2.5×10^6
N	0	0	0.28	6.2×10^3	0.37	8.1×10^3
O	0	0	1.40	2.7×10^4	1.86	3.6×10^4

[a] The number of atoms is estimated based on the number of C atoms (2.5×10^6) of a spherical ND (30 nm in diameter).

decreases the C content, because aminododecanoate has the following molecular formula: $C_{12}H_{24}NO_2$ (C, 67.2%; H, 11.3%; N, 6.5%; and O, 14.9% (by weight)). In comparison with **6-A**, the H and N contents in **6-B** are larger, but the C content is less, indicating clearly that **6-B** is covered more densely with aminododecanoate groups than **6-A**. This is consistent with the result of IR spectra (Figure 1), as described above; route B gave better coverage than route A, despite the three-step process. The reaction was reported to occur between carboxylic acid and the radical formed by hydrogen abstraction from the surface of **1** by benzoyl radical (PhCOO·) generated from benzoyl peroxide (BPO).[44,45] Therefore, the protection of the amino group with Boc may suppress the formation of the twitter ion ($^-_2OC(CH_2)_{11}NH_3^+$), accelerating the reaction of the ND radical with the amino acid. In addition, the Boc group increases the solubility of the reactant in DMF, facilitating the radical reaction.

If the functionalized ND (30 nm in diameter) has a spherical shape, each particle is calculated to consist of 2.5×10^5 C atoms.[79] Based on the number of C atoms in the ND core and the result of elemental analysis, the numbers of H, N, and O atoms can be estimated as shown in Table 1. The number of N atoms corresponds to that of the aminododecanoate introduced to the ND, because each functional group includes only one N atom ($C_{12}H_{24}\underline{N}O_2$) and nitrogen is not detected in **1**. The ratio of the numbers of N atoms in **6-A** and **6-B** ($8.1 \times 10^3/6.2 \times 10^3 = 1.3$) indicates that **6-B** is functionalized with aminododecanoate 30% more than **6-A**. The numbers of H atoms increased from that in **1** are 1.5×10^5 in **6-A** and 1.9×10^5 in **6-B**. These numbers are almost equal to those derived by multiplying the corresponding number of N atoms by 24, which corresponds to the number of H atoms in aminododecanoate ($C_{12}\underline{H_{24}}NO_2$). Approximately 30% more coverage with the functionality in **6-B** is also confirmed by the ratio of these numbers ($1.9 \times 10^5/1.5 \times 10^5 = 1.3$). On the other hand, the actual numbers of O atoms in **6-A** and **6-B** are larger than those estimated from the number of N atoms. This is probably because the radical generated on the ND also reacted with the water originally included in commercial BPO and with the benzoic acid generated in situ through the abstraction of hydrogen by benzoyl radical, giving hydroxyl and benzoate groups, respectively.

Synthesis and Characterization of Fluorescent ND. Fluorescent ND **7** was synthesized via the reaction of **5** with fluorescein succinimidyl ester, as shown in Scheme 3.

(79) Shenderova, O. A.; Zhirnov, V. V.; Brenner, D. W. *Crit. Rev. Solid State Mater. Sci.* **2002**, *27*, 227–356.

Scheme 3. Synthesis of Fluorescent ND 7 from 5

Because of the solubility in dimethyl sulfoxide (DMSO), the ammonium salt **5** was used under basic conditions. The immobilization of the fluorescent tag was confirmed by fluorescence microscopy and spectroscopy, as shown in Figures 3a and 3b, respectively, as well as ^{1}H NMR spectroscopy in Figure S3 in the Supporting Information. Bright green light was emitted from the ND particles, which appear as black dots in the bright-field image (see Figure 3a). In addition, the emission at 540 nm was confirmed in the fluorescence spectrum of a DMSO dispersion of **7** at an excitation of 490 nm. The fluorescence wavelength of **7** is 10 nm shorter than that of succinimidyl ester of fluorescein under similar conditions in the fluorescence spectra shown in Figure 3b. This is probably due to the immobilization of the fluorescein onto the ND surface. In the ^{1}H NMR spectrum of **7** dispersed in DMSO-d_6 (see Figure S3 in the Supporting Information), multiple signals were observed in the aromatic region (6.5−8.4 ppm), where no signals were detected before the immobilization of fluorescein. The resonance of $−CO_2\underline{H}$ in fluorescein (see Scheme 1) was also observed as a broad signal at 10.2 ppm. On the IR spectrum of **7** (Figure S4 in the Supporting Information), absorption due to aromatic C−C bonds was appeared at ~ 1600 cm^{-1}, whereas no such peaks were observed on the spectrum of **6-B**. These observations support the immobilization of fluorescein on the ND surface.

According to the molecular design mentioned above, the amino group apart from the ND surface formed an amide linkage with fluorescein, immobilizing the fluorescent tag covalently on the ND. Fluorescent ND was successfully obtained through the multistep organic transformations on the ND surface.

Synthesis, Characterization, and Biological Application of Fluorescent ND Dispersible in a Buffer Solution. For biomedical application of thus-synthesized ND, the fluorescent particle must be stably dispersed under a physiological environment. Therefore, a polyethylene glycol (PEG) moiety was designed to be introduced between the aminododecanoate and the fluorescent tag in **7** to add sufficient hydrophilicity for the ND to be

dispersed in PBS and cell culture medium. Surface functionalization to produce stable hydrosols is raised as a key aspect for biomedical application of ND in the very recent reviews.[61,63] To add hydrophilic functionality to the ND, we extend the concept of "functionalization partitioning" proposed by Dai from two dimensional (2D) to three dimensional (3D).[23] The functionalization partitioning of
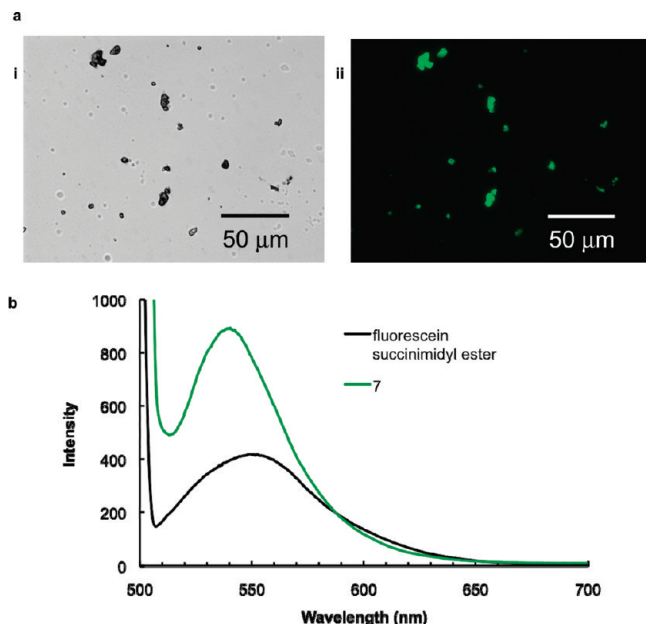

Figure 3. Characterization of fluorescent ND **7**: (a) bright-field image of **7** (panel i) and fluorescence image of **7** (panel ii) at an excitation of 470−490 nm and an emission of 515−550 nm, and (b) fluorescence spectra of **7** and fluorescein succinimidyl ester (Scheme 1) in DMSO at an excitation of 490 nm.
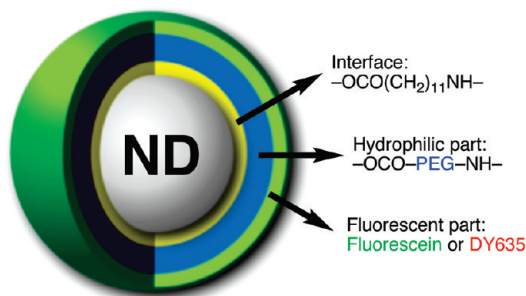

Figure 4. Schematic representation of the layered structure of fluorescent ND stably dispersed under a physiological environment.

carbon nanotubes was realized by imparting multiple functions at the different areas on the wide surface of carbon nanotubes.[23] On the other hand, the requisite functions are partitioned to the covalently connected layers above the ND surface in our case. A schematic representation of our 3D functionalization partitioning is shown in Figure 4. The functionalized ND designed here consists of four layers including the core, interfacial, hydrophilic, and luminescent segments from the center to the periphery. Since the surface area in one ND particle is not as large as that in a carbon nanotube, the 3D model is considered to be rational for the design of multifunctional ND.

The dispersible fluorescent ND was synthesized through multistep transformations of ND, shown in Scheme 4. The ammonium salt **5** was converted to **8** by reacting under basic conditions with N-Boc-ω-amino acid derivative (molecular weight: ca. 5000) possessing PEG in the body and succinimidyl ester at the C-terminus. The introduction of PEG to **5** and the deprotection of Boc group in **8** were confirmed by solution-phase ^{1}H NMR and ^{13}C NMR, as shown in Figure 5 and Figure S5 (see the Supporting Information), respectively. With regard to the ^{1}H NMR spectra of **8** and **9** shown in Figure 5, the hydrogens at PEG ($-OC\underline{H}_2C\underline{H}_2O-$) and dodecanoate ($-C\underline{H}_2-$) were observed at 3.5 and 1.2 ppm, respectively, as singlets. However, the intensities of these resonances are largely different, because one PEG chain includes more than 100 ethylene oxide units ($-CH_2CH_2O-$), corresponding to more than 400 hydrogens, which are much more than the number of hydrogens in a dodecanoate moiety ($-CH_2-$). After the reaction of **8** in trifluoroacetic acid, the resonance corresponding to t-Bu at 1.35 ppm disappeared on the spectrum of **9**, which is indicative of deprotection of the Boc group in **8**. The downfield shift of the water signal from 3.3 ppm to 3.8 ppm supports the conversion of the Boc-protected amino group ($-NH$-Boc) to ammonium ($-NH_3^+$), because the proton from the ammonium is considered to cause the downfield shift of water in DMSO-d_6. In the ^{13}C NMR spectra of **8** and **9** shown in Figure S5 (see the Supporting Information), the resonance of PEG was observed at 70 ppm. The signal of the ND core was observed at 34 ppm[72] only in the spectrum of **9**, probably because of its higher solubility in DMSO. The solution-phase NMR spectroscopies

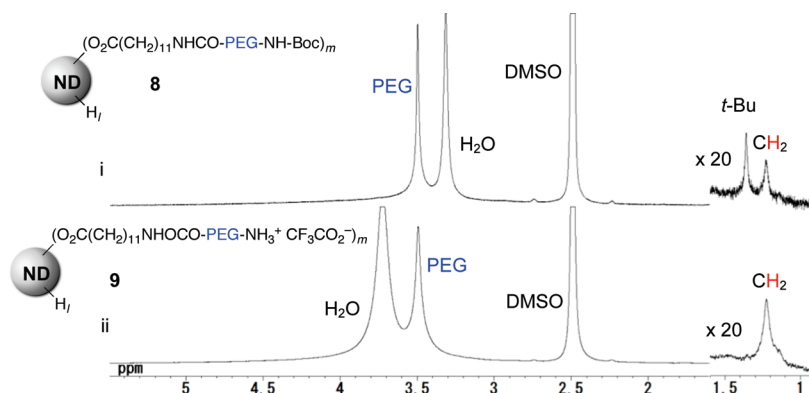**Scheme 4. Synthesis of Fluorescent ND 10 from 5.**
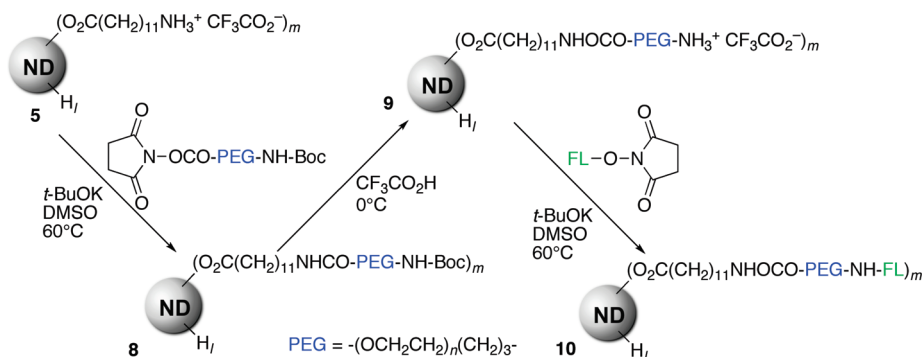
Figure 5. Solution-phase ^{1}H NMR spectra of **8** (spectrum i) and **9** (spectrum ii) in DMSO-d$_6$. The range of 0.9−1.6 ppm was expanded vertically by a factor of 20 to clarify the relatively small resonances.
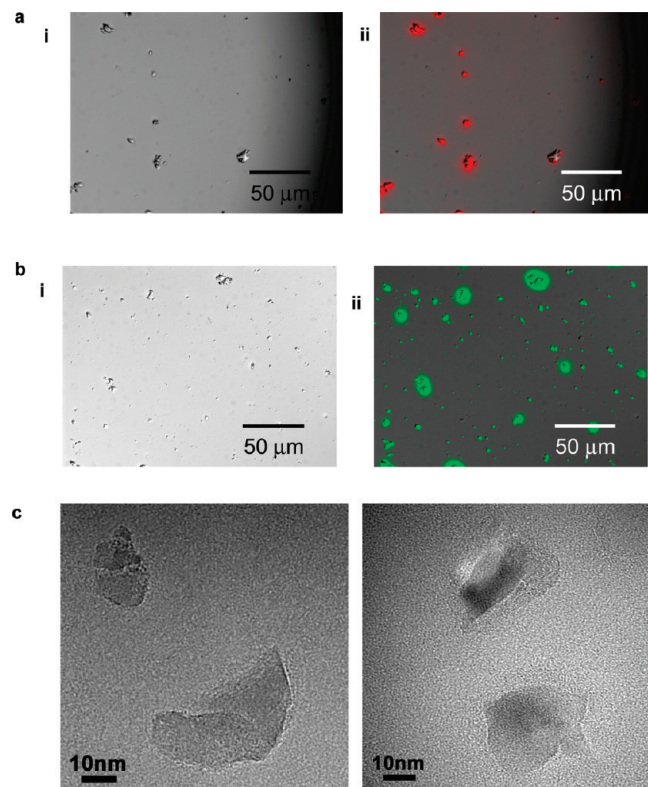

Figure 6. (a) Bright-field image (panel i) and fluorescence image (panel ii) of **10**, including DY635 as fluorescent tag instead of fluorescein, at an excitation of 630−650 nm and an emission of 671−693 nm, after merging with the bright-field image (panel i). (b) Bright-field image (panel i) and fluorescence image (panel ii) of **10**, at an excitation of 470−490 nm and an emission of 515−550 nm, after merging with the bright-field image (panel i). (c) TEM images of **10**.

Table 2. Particle Size Analyses of Starting ND, 5, and 10

	starting ND[a]	5[b]	10[b]
median diameter (nm)	30	37	48

[a] ND provided by Tomei Diamond Co., Ltd. [b] Structures are depicted in Scheme 4.
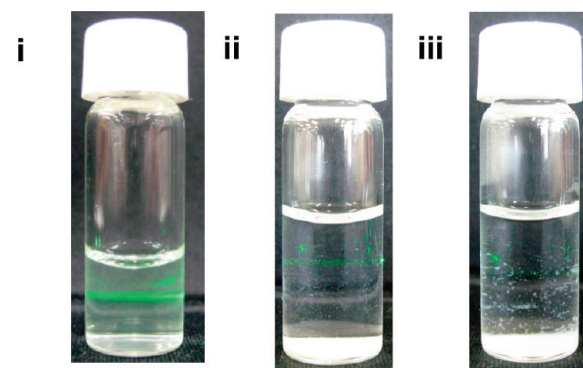

Figure 7. (i) PBS dispersion of **10** after more than one month, still exhibiting a clear Tyndall effect with green laser light. (ii) An aqueous solution (0.5 mL) of ND 30 nm in diameter, which was treated with mixed acid (H$_2$SO$_4$/HNO$_3$), was allowed to stand at room temperature for one day after the addition to PBS (2.0 mL), showing almost no ND in the solution phase. (iii) An aqueous solution (0.5 mL) of detonation ND (5 nm in diameter) was allowed to stand at room temperature for one day after the addition to PBS (2.0 mL), showing almost no ND in the solution phase.

support the organic transformations of **5 → 8 → 9** that are shown in Scheme 4. In the IR spectra shown in Figure S6 (see the Supporting Information), the existence of PEG was unambiguously confirmed in both **8** and **9**, because of the characteristic absorption of C−O and C−H stretching at 1100 and 2850 cm^{-1}, respectively. However, deprotection of the Boc group did not give any clear change on the IR spectrum, showing the limitation of IR spectroscopy for structural characterization. This is in marked contrast to the ^{1}H NMR spectroscopy shown in Figure 5, where the signal due to the *t*-butyl group

disappeared after deprotection. In the final step, fluorescein was immobilized through amide linkage in a manner similar to that in the synthesis of **7** (see Scheme 3), providing **10**. The fluorescent tag emitting red light (DY635) was also bound to **9** in the same procedure, which was confirmed by fluorescence microscopy, as shown in Figure 6a.

Product **10** was analyzed with fluorescence microscopy (Figure 6b), fluorescence spectroscopy (Figure S7 in the Supporting Information), and transmission electron microscopy (TEM) (Figure 6c and Figure S8 in the Supporting Information). Fluorescence was observed in the fluorescence microscopy (Figure 6b(ii)) from the dots in the bright-field image (Figure 6b(i)), indicating that the functionalized ND emits fluorescence. Fluorescence at 518 nm was confirmed by an excitation at 490 nm in the
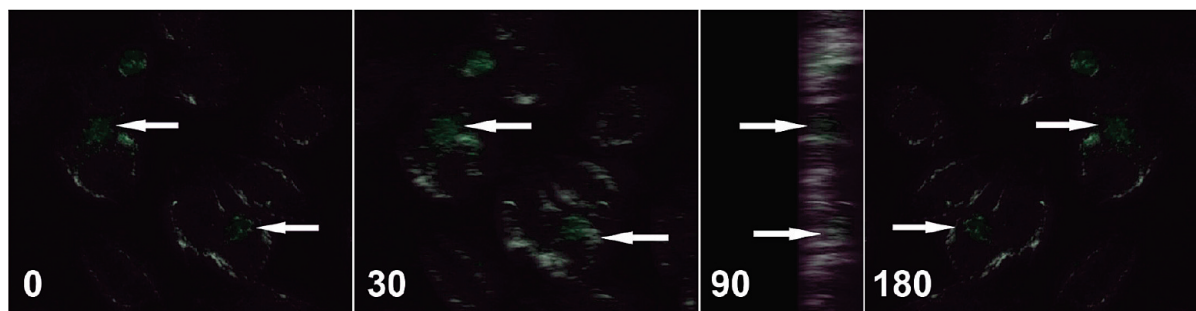
Figure 8. 3D images of HeLa cells at different angles after introduction of fluorescent ND **10**. The 3D image with a depth of 17 μm at 0° (left) was rotated by 360° around the vertical axis, as shown in the video presented in the Supporting Information. The images at 0°, 30°, 90°, and 180° are demonstrated here. The arrows in these images indicate the green fluorescence emitted from the NDs at the two positions.

fluorescence spectroscopy of **10** dispersed in PBS (shown in Figure S7 in the Supporting Information). TEM images (Figure 6c and Figure S8 in the Supporting Information) show that the particles have a variety of sizes (20−60 nm) and shapes. The median diameter of the particle was also confirmed by particle size analysis and was determined to be 48 nm (see Figure S9a in the Supporting Information). The median diameter of **10** is slightly larger than those of the starting ND (Figure S9b in the Supporting Information) and **5** (Figure S9c in the Supporting Information), as shown in Table 2, because of the coverage of ND with long chains including PEG groups. Although **7** is only dissolved in a few organic solvents (such as DMF and DMSO), **10** is stably dispersed not only in water, but also in PBS (see Figure 7i). Hydrophilicity of the PEG group remarkably increased the dispersibility of **10** and realized stable dispersion of the ND in PBS, although the dispersibility is not very high. The amount of ND dispersed in PBS was determined to be ~0.04 mg/mL. Since the dispersibility may be proportional to the number of PEG groups on the ND surface, it should increase by further optimization of the reaction conditions, enabling the immobilization of more PEG groups. On the other hand, NDs treated with a mixed acid (mixture of concentrated H_2SO_4 and HNO_3) at high temperature have been reported to have good dispersibility in water, but they are not dispersible in PBS, as shown in Figures 7ii and 7iii.[59,61,62,80]

Since **10** was also dispersed in the medium used for cell culture, we applied thus-synthesized ND to cell labeling. At the first attempt, HeLa cells were simply incubated in the presence of **10** in the culture medium. However, no introduction of **10** into the cells was observed upon fluorescence microscopy, probably because of the high dilution of **10**. Therefore, the complex of **10** with the hemagglutinating virus of Japan envelope (HVJ-E) was prepared and then applied to cell incubation. After 70 h, the cells were fixed on a chamber slide, washed with PBS, and observed using a confocal laser-scanning microscope. As shown in the 3D images of the cells (Figure 8) and the video presented in the Supporting Information, **10** was unambiguously introduced into the HeLa cells. The fluorescence originating from **10** was observed in the

perinuclear cytoplasmic vesicles, suggesting that **10** was incorporated into the endocytic vesicles.

For more biomedical applications of the ND, targeting specificity could be also incorporated in **10** by adding one more outer conjugate shell that possesses peptides such as RGD (Arg-Gly-Asp) and LFPLH (Leu-Phe-Pro-Leu-His) or replacing some of the fluorescent tag to the peptides in the outmost layer in **10**.[81,82]

Conclusion

We have shown that multiple steps of organic transformation and characterization sequence constructed nanodiamond (ND) with multifunctions, including fluorescence and dispersibility under a physiological environment. First, ω-aminododecanoic acid was immobilized as the interface between the ND surface and the subsequent functionality, because direct introduction of bulky functionality is considered to be difficult. The ω-aminododecanoate of the ND was well-characterized by IR, solution-phase NMRs, and elemental analysis. The hydrophilic and fluorescent segments including PEG and fluorescein or DY635, respectively, were introduced successively through the amide linkages. These organic transformations on the ND surface enabled the assembly of fluorescent ND stably dispersed under a physiological environment. The fluorescent and hydrophilic functions are partitioned to the two outermost layers of the ND. The ND thus synthesized was introduced into HeLa cells, which was imaged fluorescently. In principle, more functions such as targeting specificity and more imaging modalities can be incorporated into ND by extending the outer layer (in other words, by expanding the concept of the 3D partitioning functionalization).

Experimental Section

Materials. ND powder with a median diameter of 30 nm is prepared by size-separating the powdered diamond from the bulk synthesized by a static high-pressure high-temperature (HPHT) method; it was kindly provided by Tomei Diamond Co., Ltd.[83] Detonation ND (5 nm in diameter), used in Figure 7iii, is

(80) Neugart, F.; Zappe, A.; Jelezko, F.; Tietz, C.; Boudou, J. P.; Krueger, A.; Wrachtrup, J. *Nano Lett.* **2007**, *7*, 3588–3591.

(81) Liu, Z.; Tabakman, S.; Welsher, K.; Dai, H. *Nano Res.* **2009**, *2*, 85–120.

(82) Liu, Z.; Cai, W.; He, L.; Nakayama, N.; Chen, K.; Sun, X.; Chen, X.; Dai, H. *Nature Nanotechnol.* **2007**, *2*, 47–52.

(83) Morita, Y.; Takimoto, T.; Yamanaka, H.; Kumekawa, K.; Morino, S.; Aonuma, S.; Kimura, T.; Komatsu, N. *Small* **2008**, *4*, 2154–2157.

purchased from NanoCarbon Research Institute Co., Ltd.[84] Hydrogenated ND **1** and aminated ND **2** were prepared by Tomei Diamond Co., Ltd., according to the reported procedure.[74,75] Succinimidyl ester of fluorescein was purchased from Thermo Fisher Scientific, Inc. Boc-protected aminododecanoic acid was prepared from ω-aminododecanoic acid (Wako Pure Chemical Industries, Ltd.) and di-*t*-butyl dicarbonate (Wako Pure Chemical Industries, Ltd.). Commercial benzoyl peroxide (BPO), including 25% water (Nacalai Tesque, Inc.), was used for the radical reaction without purification. The ND **5** was PEGylated using commercial α-3-(*N*-*t*-butyloxycarbonylamino)propyl-ω-(succinimidyloxycarboxy), polyoxyethylene (SUNBRIGHT BO-050TS, NOF Co.). All other reagents and solvents were purchased from commercial sources and used without purification.

Equipments. IR spectral measurements were conducted using IR Prestige-21 (Shimadzu Co.). [1]H (270 MHz) and [13]C (67.5 MHz) NMR spectra were recorded on a JEOL Model JNM-EX270 spectrometers. The relaxation times were calculated using the EXcalibur program for Windows (version 4.1). Particle size analysis was performed on a Nanotrac UPA-UT151 system (Microtrac, Inc.). Fluorescence spectra were measured on an F-4500 (Hitachi, Ltd.). Fluorescence and bright-field images were obtained with a BX61 system (Olympus Co.). Three-dimensional images of the cells were obtained with a confocal laser-scanning microscope (C1si, Nikon Co.). Elemental analyses of CHN and O were performed at Integrated Center for Sciences, Ehime University and on a VarioMICRO-cube (Elementar Analysensysteme GmbH), respectively.

Synthesis of 6-A from 1. Aminododecanoic acid (381 mg, 1.77 mmol) and BPO (105 mg, 0.432 mmol) were added to a suspension of **1** (40.1 mg) in DMF (10 mL). After the suspension was sonicated at 75 °C for 2 h, a 1:1 mixture of ethyl acetate: hexane (60 mL) was added to the suspension. Filtration followed by washing with acetic acid, triethylamine, water, and methanol gave 41.1 mg of black solid, which was characterized by IR (see Figure 1).

Synthesis of 4 from 1. To a suspension of **1** (0.800 g) in DMF (200 mL) were added *N*-Boc-ω-aminododecanoic acid (11.2 g, 35.4 mmol) and BPO (2.06 g, 8.52 mmol). After the suspension was sonicated at 75 °C for 2 h, a 1:1 mixture of ethyl acetate: hexane (60 mL) was added to the suspension. The solid was recovered from the suspension by centrifugation at 18 500 *g* several times and was washed with ethyl acetate, triethylamine, water, and methanol, giving 0.823 g of black solid. The product was characterized by ^{1}H NMR (see Figure 2) and ^{13}C NMR (see Figure S2 in the Supporting Information).

Deprotection of Boc from 4. A suspension of **4** in trifluoroacetic acid (1.0 mL) was stirred at 0 °C for 5 min. After adding chloroform, the suspension was centrifuged at 18 500 *g*. The precipitates were washed with chloroform several times and dried in vacuo, giving black solid **5** (16.2 mg). After washing with triethylamine, the amine **6-B** was characterized by IR (see Figure 1).

Synthesis of Fluorescent ND 7 from 5. Succinimidyl ester of fluorescein (2.02 mg, 4.27 μmol) and potassium *t*-butoxide (1.04 mg, 9.27 μmol) were added to a suspension of **5** (10.0 mg) in dry DMSO (0.15 mL). After stirring at room temperature for 2 h under argon atmosphere, the reaction was quenched by the addition of diethyl ether (10 mL) and the reaction mixture was filtered. The recovered solid was washed with triethylamine/methanol, methanol, and water, and dried in vacuo to give black solid **7** (9.55 mg).

The fluorescent ND was characterized by fluorescence microscopy (see Figure 3a) and spectroscopy (see Figure 3b), ^{1}H NMR (see Figure S3 in the Supporting Information) and IR (see Figure S4 in the Supporting Information).

Synthesis of Fluorescent ND 10 from 5. To a suspension of **5** (0.100 g) in dry DMSO (1.50 mL) were added α-3-(*N*-*t*-butyloxycarbonylamino)propyl-ω-(succinimidyloxycarboxy)polyoxyethylene (0.300 g, 63.1 μmol) and potassium *t*-butoxide (10.0 mg, 89.2 μmol). The resulting suspension was stirred at 60 °C for 18 h under argon atmosphere. After adding diethyl ether (10 mL), the suspension was filtered, and the solid was washed with triethylamine/methanol, methanol, and water. Black solid **8** (96.8 mg) was obtained after drying in vacuo.

Deprotection of the Boc group was accomplished by adding **8** (50.0 mg) in trifluoroacetic acid (1.0 mL). After stirring at 0 °C for 5 min, the reaction was quenched by the addition of chloroform (15 mL), and the resulting suspension was centrifuged at 18 500 *g*. The recovered solid was washed with chloroform and dried in vacuo to give black solid **9** (38.4 mg). ^{1}H NMR and ^{13}C NMR studies, as well as IR spectroscopy of **8** and **9** are shown in Figures 5, S5 (in the Supporting Information), and S6 (in the Supporting Information), respectively.

Succinimidyl ester of fluorescein (5.02 mg, 3.17 μmol) and potassium *t*-butoxide (0.80 mg, 7.13 mmol) were added to a suspension of **9** (5.02 mg) in dry DMSO (0.12 mL). After stirring at 60 °C for 18 h under an argon atmosphere, the reaction was quenched by the addition of diethyl ether (6.0 mL), and the reaction mixture was filtered. The recovered solid was washed with triethyl amine/methanol, methanol, and water, and then it was dried in vacuo to give black solid **10** (4.06 mg). Fluorescence from ND was confirmed by fluorescence microscopy (see Figure 6b) and spectroscopy (see Figure S7 in the Supporting Information).

Introduction of Fluorescent ND 10 into Cultured HeLa Cells. HeLa cells (5×10^4 cells per well in 4-well LabTek chamber slides [BD bioscience]) cultured in Dulbecco's modified Eagle's medium (DMEM) containing 10% fetal bovine serum were incubated for 70 h with the complex between the hemagglutinating virus of Japan envelope (HVJ-E) and fluorescent ND **10**. The complex was prepared using HVJ-E transfection kit (GenomONE, Ishihara Sangyo Kaisha, Ltd.) according to the supplier's recommendations and was applied to cell incubation at a concentration of ~1 μg/mL of **10**. The cells were fixed with 1% buffered formaldehyde and 70% ethanol, washed with PBS, and mounted with glycerol. Both optical and fluorescent images of the cells were obtained under identical conditions using a confocal laser-scanning microscope and overlapped to prepare the 3D images (see Figure 8) and the video provided in the Supporting Information. The 3D image was composed of 27 scan images to a depth of 17 μm.

(84) Krüger, A.; Kataoka, F.; Ozawa, M.; Fujino, T.; Suzuki, Y.; Aleksenskii, A. E.; Vul', A. Y.; Osawa, E. *Carbon* **2005**, *43*, 1722–1730.

Supporting Information Available: Bright-field and fluorescent images of **3**, and infrared spectra of **2** and **3** (Figure S1). Solution-phase ^{13}C NMR of **4** and *N*-Boc-ω-aminododecanoic acid in CDCl$_3$ (Figure S2) and solution-phase ^{1}H NMR spectra of **7** in DMSO-d$_6$ (Figure S3). Infrared spectra of **6-B** and **7** (Figure S4). Solution-phase ^{13}C NMR of **8** and **9** in DMSO-d$_6$ (Figure S5). Infrared spectra of **6-B**, **8**, and **9** (Figure S6). Fluorescence spectrum of **10** dispersed in PBS (Figure S7). TEM photomicrographs of **10** (Figure S8). Particle size analyses of **10** dispersed in PBS, the starting ND dispersed in water, and **5** dispersed in DMSO (Figure S9). (PDF) Video showing rotating 3D imaging of HaLa cells, in which **10** was introduced. This material is available free of charge via the Internet at http://pubs.acs.org.